PCCP

Physical Chemistry Chemical Physics

www.rsc.org/pccp

Volume 12 | Number 5 | 7 February 2010 | Pages 1009–1204

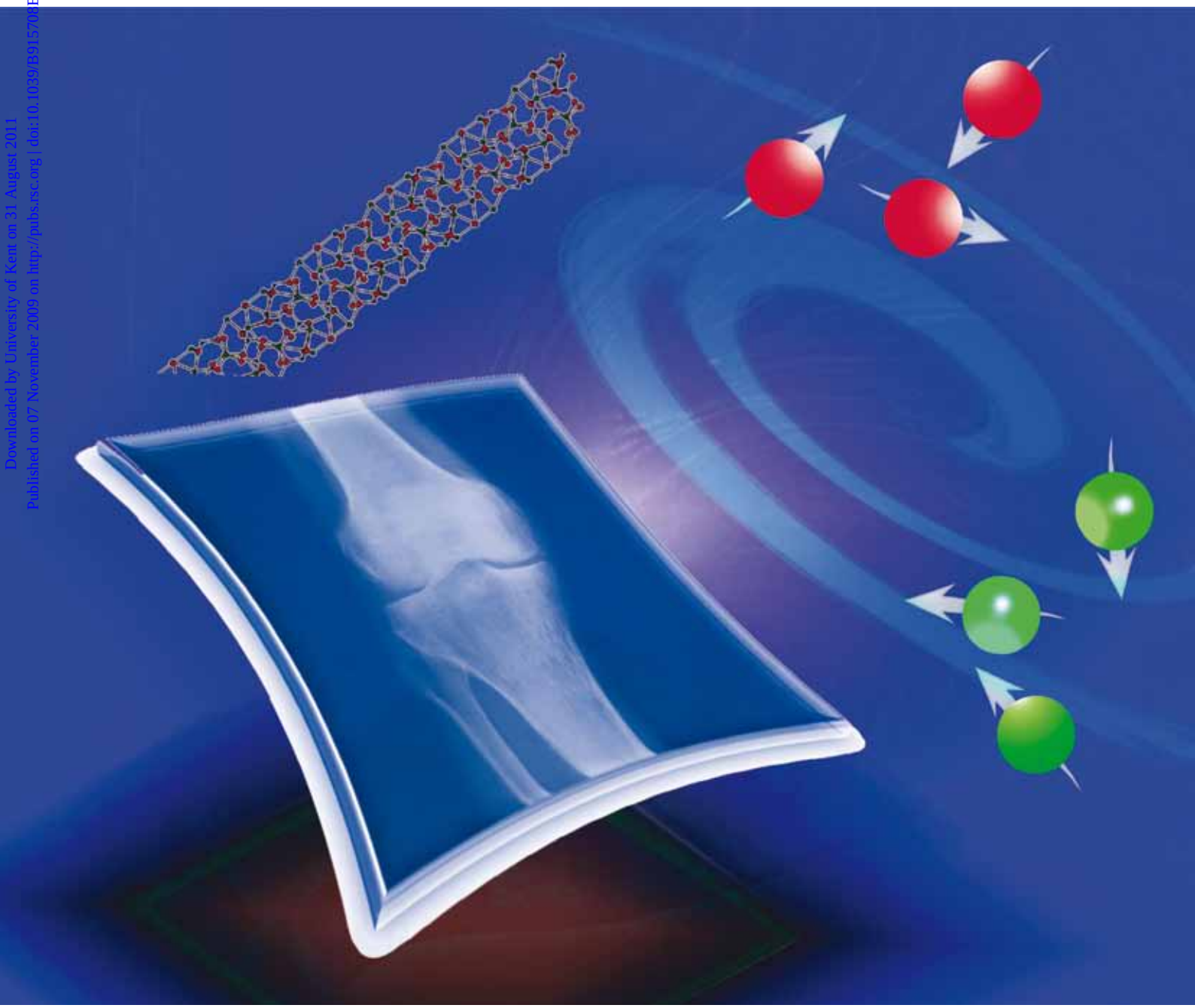

ISSN 1463-9076

COVER ARTICLE
Laurencin *et al.*
Probing the calcium and sodium local environment in bones and teeth using multinuclear solid state NMR and X-ray absorption spectroscopy

HOT ARTICLE
Lewerenz and Slavíček
Snowballs, quantum solvation and coordination: lead ions inside small helium droplets

1463-9076(2010)12:5;1-T

Probing the calcium and sodium local environment in bones and teeth using multinuclear solid state NMR and X-ray absorption spectroscopy†

Danielle Laurencin,‡*[a] Alan Wong,§[a] Wojciech Chrzanowski,[b] Jonathan C. Knowles,[b] Dong Qiu,¶[c] David M. Pickup,[c] Robert J. Newport,[c] Zhehong Gan,[d] Melinda J. Duer[e] and Mark E. Smith*[a]

Received 31st July 2009, Accepted 5th October 2009
First published as an Advance Article on the web 7th November 2009
DOI: 10.1039/b915708e

Despite the numerous studies of bone mineral, there are still many questions regarding the exact structure and composition of the mineral phase, and how the mineral crystals become organised with respect to each other and the collagen matrix. Bone mineral is commonly formulated as hydroxyapatite, albeit with numerous substitutions, and has previously been studied by ^{31}P and ^{1}H NMR, which has given considerable insight into the complexity of the mineral structure. However, to date, there has been no report of an NMR investigation of the other major component of bone mineral, calcium, nor of common minority cations like sodium. Here, direct analysis of the local environment of calcium in two biological apatites, equine bone (HB) and bovine tooth (CT), was carried out using both ^{43}Ca solid state NMR and Ca K-edge X-ray absorption spectroscopy, revealing important structural information about the calcium coordination shell. The ^{43}Ca δ_{iso} in HB and CT is found to correlate with the average Ca–O bond distance measured by Ca K-edge EXAFS, and the ^{43}Ca NMR linewidths show that there is a greater distribution in chemical bonding around calcium in HB and CT, compared to synthetic apatites. In the case of sodium, ^{23}Na MAS NMR, high resolution 3Q-MAS NMR, as well as ^{23}Na{^{31}P} REDOR and ^{1}H{^{23}Na} R^{3}-HMQC correlation experiments give the first direct evidence that some sodium is located inside the apatite phase in HB and CT, but with a greater distribution of environments compared to a synthetic sodium substituted apatite (Na-HA).

[a] *Department of Physics, University of Warwick, Coventry, UK CV4 7AL. E-mail: danielle.laurencin@univ-montp2.fr, M.E.Smith.1@warwick.ac.uk*
[b] *Eastman Dental Institute, University College London, 256 Gray's Inn Road, London, UK WC1X 8LD*
[c] *School of Physical Sciences, Ingram Building, University of Kent, Canterbury, UK CT2 7NR*
[d] *Center of Interdisciplinary Magnetic Resonance, National High Magnetic Field Laboratory, Tallahassee, Florida, FL32310, USA*
[e] *Department of Chemistry, University of Cambridge, Lensfield Road, Cambridge, UK CB2 1EW*

† Electronic supplementary information (ESI) available: A—Background characterisation of HB, CT, HA and Na-HA: Fig. S1: IR spectra and XRD powder patterns. Fig. S2: ^{13}C{^{1}H} CPMAS NMR spectra of HB and CT. Fig. S3: ^{1}H and ^{31}P MAS NMR spectra of HA, Na-HA, HB and CT. Fig. S4: ^{1}H{^{31}P} CPMAS spectrum of HB. Table S1: Na/Ca molar ratios in Na-HA, HB and CT, as determined by ICP-MS. B—Additional analyses of the calcium environment in HB, CT and synthetic models: Fig. S5: ^{43}Ca MAS NMR spectra of Na-HA, HB and CT at different magnetic fields. Fig. S6: ^{43}Ca MAS NMR spectra of HA, Na-HA, CT and fluoroapatite at 19.6 T. Table S2: Fitting parameters of the Ca K-edge EXAFS data of HA, CT and HB. Fig. S7: Natural-abundance ^{43}Ca{^{1}H} REDOR NMR spectra of HB. C—Additional analyses of the sodium environment in HB, CT and Na-HA: Fig. S8: ^{23}Na MAS NMR spectra of Na-HA, HB and CT at different magnetic fields. Fig. S9: ^{23}Na{^{1}H} 3Q-REDOR study of Na-HA. See DOI: 10.1039/b915708e

‡ Current address: Institut Charles Gerhardt de Montpellier, UMR 5253, CNRS-UM2-ENSCM-UM1, Université de Montpellier 2, CC 1701, Place Eugène Bataillon, 34095 Montpellier cedex 5, France.
§ Current address: CEA Saclay, IRAMIS/SCM/LSDRM, Gif-sur-Yvette 91191, France.
¶ Current address: Beijing National Laboratory for Molecular Sciences, State Key Laboratory of Polymer Physics and Chemistry, Chinese Academy of Sciences, Beijing 100190, China

Introduction

Bone, tooth enamel and dentin are naturally occurring biominerals, consisting of an organic matrix (primarily collagen type I) on which are deposited nanocrystals of a mineral phase commonly formulated as hydroxyapatite (HA).[1,2] In bone, the mineral crystals are mainly plate-like in morphology, around 2–4 nm thickness, and with highly variable width and length (averaging 25 × 50 nm). Their size, shape, morphology, crystallinity and composition vary markedly with crystal age as bone remodels continuously, and the *degree* of mineralisation varies throughout a single bone.[3] More recently, it has been shown that in addition to these plate-like structures, spherical to cylindrical mineral crystals occur in bone with diameters of around 20 nm.[4] In tooth dentin and enamel, the mineral crystals are generally somewhat larger and exhibit greater crystallinity.

On the nanoscale, bone and teeth are highly organised materials. The plate-like crystals are mainly arranged in parallel arrays, occupying the hole zones between the ends of cross-linked, triple helical collagen molecules and between collagen fibrils; it is estimated that there are around four collagen molecules between each mineral crystal layer.[5] Despite the numerous studies of bone mineral, there are still many questions regarding how bone mineral forms, how the mineral crystals become organised with respect to each other and the collagen matrix, and about the morphology and

distribution of mineral crystals within the collagen network.[3] With respect to the latter question, most studies utilise electron microscopy in some form.[6,7] However, the harsh conditions required for sample preparation are problematic when dealing with nanocrystalline materials like bone. Indeed, it is to be noted that the majority of these studies required the initial removal of the entire organic matrix from the sample and/or several dehydration steps, meaning that the material analysed under the electron beam might have undergone structural modifications. There is thus a great need for spectroscopic methods capable of studying the *local* structure and environment of the inorganic phase in intact samples.

At the atomic level, the complexity of the mineral phase of bone and teeth is further increased due to the presence of many minority ions, such as CO_3^{2-}, F^-, Na^+ and Mg^{2+}.[8–10] The actual composition of biological apatites is thus different from that of synthetic hydroxyapatite $Ca_{10}(PO_4)_6(OH)_2$ (Fig. 1), and is often referred to as carbonated apatite, due to the generally high CO_3^{2-} content. The relative proportions of the different minority ions are variable, depending for example on the part of the tissue sampled and its age.[8,10] Although they are present in very small quantities, these ions often have a strong influence on the functional properties of bone and teeth. For example, sodium plays a role in bone remodeling,[11] magnesium deficiency leads to an increase in osteoclastic bone resorption,[12] and fluoride helps prevent the development of dental caries.[13]

Infra-red (IR) spectroscopy,[14–16] XRD,[17,18] and X-ray absorption spectroscopy,[19–21] have played their part in unravelling the complexity of the mineral structure. However, even greater insight has come from NMR studies. The first solid state NMR studies of bone and teeth tissues were performed more than 20 years ago,[22,23] but with improvements in methodology over the past few years, NMR has started to emerge as a key analytical tool for these materials.[24] Studies using ^{31}P and/or ^{1}H nuclei[16,22–43] have shown that the mineral particles are overall highly heterogeneous in structure, a feature which is likely to be key in the structural role they play within the biomineral. Furthermore, using ^{31}P–^{1}H correlation experiments, a small quantity of HPO_4^{2-} anions[22,29,35–38] in the surface regions of the mineral particles was evidenced, as well as an apparent lack of hydroxyl groups (OH^-) in the mineral phase relative to the ideal apatite structure.[26,39] NMR studies have also revealed that water has several different structural roles in the mineral,[40,41] and have allowed the local environment around minority anions like F^- and CO_3^{2-} to be analysed.[23,44–47] More recently, ^{13}C–^{31}P correlation experiments have suggested that glycosaminoglycan molecules are located at the interface between the organic and mineral phases of bone and teeth.[48–50]

To the best of our knowledge, however, solid state NMR has only been used to date to probe the structural environment of the mineral *anions*: the local environment around the metal *cations* (Ca^{2+}, Mg^{2+} or Na^+...) in the mineral structure has not yet been investigated by NMR. Clearly, this represents a huge gap in the characterization of the mineral structure. This is not surprising in the case of calcium, the most abundant metal cation in the mineral phase, since it is a very challenging nucleus for NMR: the NMR-active isotope, ^{43}Ca, is a spin-7/2 low-γ nucleus (*i.e.* with a small magnetic moment) with low natural abundance (<0.14%).[51] Nevertheless, significant progress (notably from the point of view of instrumental advances) has made ^{43}Ca solid state NMR more accessible, and several natural abundance studies of various materials have been reported, mostly in the last 3 years.[52–60] In particular, it has been demonstrated recently that the local environment of Ca^{2+} in calcium phosphates and hydroxyapatite can readily be analysed by natural abundance ^{43}Ca solid state NMR.[52,56]

The absence of systematic studies of the local environment of sodium in natural bone and teeth is more surprising. Indeed, ^{23}Na is a spin 3/2 quadrupolar nucleus of 100% natural abundance, and many ^{23}Na solid state NMR studies of inorganic materials have been reported.[51] In addition, ^{23}Na MRI has been used to analyse the structure of biological tissues like mummified bone and cartilage,[61,62] and it has recently been shown that the local environment of sodium in

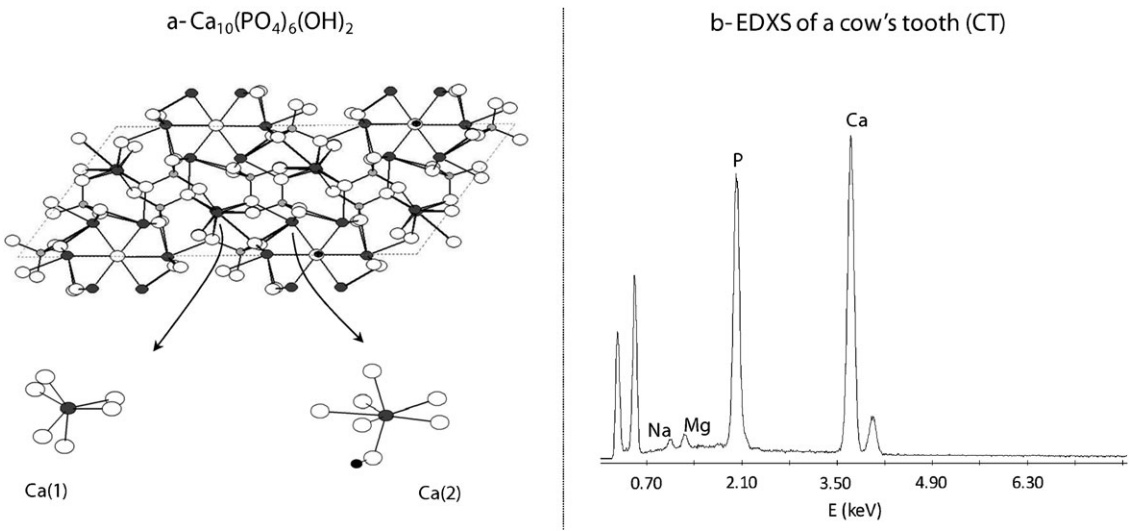

Fig. 1 (a) Representation of the crystal structure of hydroxyapatite and of the local environment around the 2 calcium sites (Ca, P, O and H atoms are in dark grey, light grey, white and black, respectively). (b) EDXS spectrum of a cow tooth sample (CT).

synthetic carbonated apatites can be studied by ^{23}Na solid state NMR.[63]

In 2005, in a review on "Solid State NMR Studies of Bone",[24] Kolodziejski concluded that "*quadrupolar nuclei like^{23}Na and^{17}O should also be considered*" and that "*the^{43}Ca resonance at natural abundance would be of great interest and could become feasible with the progress of NMR hardware*". The purpose of the present study is thus to determine how ^{43}Ca and ^{23}Na NMR can be used to analyse the local environment of calcium and sodium in bone and teeth, in view of better understanding the atomic structure of these materials, and more specifically of the mineral phase and the organic–inorganic interface. Here, we report on the ^{43}Ca and ^{23}Na NMR of equine bone (horse, referred to as HB) and bovine tooth (cow, CT) samples. Their NMR spectra are compared with those of synthetic model compounds, and discussed alongside results from complementary characterisation techniques, notably Ca K-edge X-ray absorption spectroscopy, in order to determine what information about the local structure around the cations in these materials may be gained from NMR experiments.

Experimental section

Samples studied

The horse bone (HB) and cow tooth (CT) samples were harvested from animals put down for humanitarian reasons completely unconnected with this study. They were ground into fine powders and used as such (*i.e.* without undergoing any chemical treatment). Hydroxyapatite, $Ca_{10}(PO_4)_6(OH)_2$ (HA), was synthesized by precipitation following published procedures.[64] Sodium-substituted hydroxyapatite (Na-HA)[65] and Na_3PO_4 were obtained from Aldrich. Full details of the composition and general structural features of these samples, as determined by ICP-MS, IR, XRD, ^{1}H, ^{31}P and ^{13}C magic-angle spinning (MAS) NMR, can be found in the supplementary materials (Figures S1 to S4 and Table S1, from hereon, "S" refers to data in the supplementary materials).

^{43}Ca solid state NMR

^{43}Ca solid state NMR experiments were performed on Varian Infinity 360 (8.45 T), Bruker Avance II^{+} 600 (14.1 T), Varian Infinity Plus 800 (18.8 T) and Bruker DRX 830 (19.6 T) spectrometers. Spectra were referenced to a 1 mol L^{-1} aqueous solution of $CaCl_2$ (at 0 ppm).[52] Natural abundance ^{43}Ca solid state NMR spectra were recorded at 8.45 and 14.1 T using large-rotor volume Chemagnetics-Varian probes (9.5 mm diameter MAS rotor) spinning at 4 kHz. High field measurements were performed at 18.8 T using a Varian 4 mm rotor probe spinning at 4 kHz, and at 19.6 T using a 7 mm homebuilt probe spinning at 5 kHz. Depending on the sample, recycle delays of 0.1 to 4.0 s were used, and 60 000 to 1 100 000 transients were acquired (with total experimental times ranging from 12 to 50 h). For the spectra recorded at 8.45, 14.1 and 18.8 T, the rotor-assisted population transfer (RAPT)[66,67] sequence (sets of +X/−X 2.5 μs pulses with $a \sim 15$ kHz radiofrequency field strength), which had previously been optimised for non-substituted hydroxyapatite,[56] was applied for sensitivity enhancement prior to a 90° pulse selective for the central transition. For the spectra recorded at 19.6 T, a 5 kHz chirp sweep[68] was applied for sensitivity enhancement at ~250 kHz below the central transition frequency.

Ca K-edge EXAFS and XANES

EXAFS (extended X-ray absorption fine structure) and XANES (X-ray absorption near edge structure) measurements were performed on the XAFS BL11.1 beamline at the Elettra Sincrotrone, Trieste, Italy. Samples were ground to a fine powder, diluted in polyvinyl pyrrolidone (average molecular wt 40 000, Sigma-Aldrich, "PVP40"), pressed into pellets, and run at room temperature in transmission mode using ion chambers before and after the sample to measure incident and transmitted X-ray intensity. Spectra were collected at the Ca K-edge at 4038 eV. The Elettra ring energy was 2 GeV and the current was up to 200 mA. The X-ray energy incident on the sample was defined using a two-crystal Si(111) monochromator detuned (by ~50%) to reduce high energy harmonics. The instrument was evacuated to $\sim 10^{-5}$ Pa in order to reduce X-ray losses due to attenuation in the air. An energy resolution of ~0.3 eV at the Ca K-edge was achieved, and the energy was calibrated using CaF_2 as a calibrant placed between the transmission and a third ion chamber. For the XANES spectra, the pre-edge (3900–4017 eV), edge (4017–4100 eV) and post-edge (4100–4200 eV) regions were scanned in 5.0, 0.1 and 1.0 eV steps respectively, and dwell times per point of 1.0, 2.0 and 1.0 s respectively. For the EXAFS spectra, the pre-edge (3900–4017 eV), edge (4017–4100 eV) and post-edge (4100–4800 eV) regions were scanned in 5.0, 2.0 and 1.0 eV steps respectively, and dwell times per point of 1.0, 1.0 and 2.0 s, respectively.

Data reduction was performed using the standard software packages Athena,[69] Viper2006[70] and EXCURV98.[71] Typically, two XANES and three EXAFS data sets were collected for each sample, which were respectively averaged and converted to energy using Athena. All EXAFS spectra were background subtracted using Viper2006, with a 2nd order polynomial fitted to the pre-edge region and a polynomial spline (going through 7 knots) fitted to the post-edge region to describe the underlying atomic absorption. Conversion of energy to k space followed before k^3 weighting of the data. The EXCURV98 code was then used to model the structure from the parameters of the radial shells of atoms surrounding the central atom. Phase shifts were calculated by *ab initio* curved wave theory methods in EXCURV98 for the central atom and for all backscattering elements in the samples. Multiple scattering effects were not considered for HB and CT since only the nearest coordination shells are probed at these low energies. Such a simplification has already been employed for the study of bone by Ca K-edge EXAFS spectroscopy.[20,21]

^{23}Na solid state NMR

^{23}Na solid state NMR experiments were performed on Varian Infinity Plus 300 (7.1 T), Varian Infinity 360 (8.45 T), Bruker Avance II^{+} 600 (14.1 T) and Varian Infinity Plus 800 (18.8 T) spectrometers. Spectra were referenced to solid NaCl (at 7.2 ppm). ^{23}Na MAS NMR spectra were recorded at 7.1,

8.45 and 14.1 T using Bruker 4 mm MAS probes spinning at 10 kHz, and at 18.8 T using a Varian 4 mm probe spinning at 10 kHz. 300 to 6700 transients were acquired, with recycle delays of 0.1 to 0.5 s.

^{23}Na 3Q-MAS (triple quantum-MAS)[72,73] spectra of Na-HA, HB and CT were acquired at 14.1 T on a Bruker 4 mm probe spinning at 10 kHz, using a 3Q *z*-filter experiment. The 3Q excitation and conversion pulse widths were 8 and 3 μs, respectively, with a precession rate of 100 kHz on the solid; the selective π/2 pulse used a ~20 kHz precession rate on the solid. The spectral widths were 50 kHz for both f_1 and f_2. 50 t_1 increments were recorded, with a dwell time of 20 μs. A total of 9600 transients were collected by the States method for each t_1 increment, with a recycle delay of 0.1 s. Spectra were processed using standard shearing methods.[73]

^{23}Na{^{31}P} REDOR[74,75] studies of Na-HA, HB, CT and Na_3PO_4 were performed at 14.1 T on a Bruker 4 mm MAS probe spinning at 10 kHz. ^{23}Na π/2 and π pulses of 4.0 and 8.0 μs respectively were used. ^{31}P-dephasing π pulses (of 8.25 μs) were phase cycled according to the XY-8 scheme.[76]

^{1}H{^{23}Na} R^3-HMQC (heteronuclear multiple quantum correlation)[77] spectra of Na-HA, HB and CT were recorded at 14.1 T using a Bruker 4 mm MAS probe spinning at 10 kHz. The ^{1}H π/2 and π pulses were 2.5 and 5.0 μs, respectively, and the ^{23}Na π/2 pulses were 11.5 μs. The R^3-spinlock condition[77] was set to $q = 2.0$, where $q = \nu_1/\nu_R$ (ν_1 being the rf-amplitude and ν_R the rotor frequency). Recoupling periods of 700–1100 μs were used (1100 μs for Na-HA, 700 μs for CT, and 900 μs for HB). Spectra were collected by the States method with a recycle delay of 1.0 s. The spectral widths for the f_1 (^{23}Na) and f_2 (^{1}H) dimensions were respectively 10 and 20 kHz. For the Na-HA, CT and HB, 80, 45 and 30 t_1 increments were respectively collected, with a total of 672, 1600 and 2400 scans for each t_1 increment.

Results and discussion

1 Investigation of the local environment of calcium

1a Multiple magnetic field ^{43}Ca NMR experiments. Natural abundance ^{43}Ca MAS NMR spectra of HB, CT, HA and Na-HA were recorded at different magnetic fields (Fig. 2, S5 and S6).[56] At 14.1 T, the ^{43}Ca NMR spectra of HB and CT are very similar to those of the synthetic models, with one featureless signal. At higher magnetic fields, however, differences become more noticeable. Indeed, whereas the two crystallographic calcium sites of HA and Na-HA are resolved at 18.8 and 19.6 T,[56] no analogous spectral resolution is achieved for HB and CT.

Despite the absence of defined lineshapes, two ^{43}Ca NMR parameters likely to provide information on the local environment of calcium were derived from the MAS spectra:[52,54,56] the ^{43}Ca isotropic chemical shift δ_{iso} and the ^{43}Ca quadrupolar parameter P_Q (defined as $C_Q[1 + (\eta_Q^2/3)]^{0.5}$). Using eqn (1),

$$\delta_{max} = \delta_{iso} - \left(\frac{3}{40}\right)10^6 F(I)\left(\frac{P_Q}{\nu_0}\right)^2 \qquad (1)$$

where ν_0 is the Larmor frequency of ^{43}Ca and $F(I)$ is a spin-dependent factor equal to 5/147 for $I = 7/2$, δ_{iso}, and P_Q can be extrapolated by plotting the peak maximum δ_{max} at each magnetic field against $(1/\nu_0)^2$.[78] The δ_{iso} and P_Q values of HB and CT are found to be very similar (Table 1), and in the range expected for calcium phosphates.[52,56]

1b Average Ca–O bond distance. Previous experimental and computational work on ^{43}Ca NMR has shown that the isotropic chemical shift of calcium mainly reflects the average Ca–O bond distance around the cation.[52,54,55] Therefore, the similar values of δ_{iso} for HB and CT suggest that, on average, the oxygen atoms in the first-coordination sphere around calcium are situated at the same distance in these samples. Furthermore, a first estimation of this distance can be obtained: according to our previous computational study of ^{43}Ca NMR isotropic shifts, in the case of calcium phosphates such as apatites, δ_{iso} ~ 3 ppm corresponds to an average Ca···O distance between 2.4 and 2.5 Å.[52]

These NMR results were compared to Ca K-edge EXAFS studies. The experimental EXAFS spectra $k^3\chi(k)$ and the moduli of the Fourier transforms of HB, CT and synthetic HA are shown in Fig. 3. In the case of crystalline HA, the first shells (<3 Å) correspond to the nearest oxygen neighbours, whereas the further shells arise from the scattering of various oxygen, phosphorus and calcium atoms.[79] In contrast, for HB and CT, no evidence of ordered shells is noticeable beyond ~4 Å. The loss of long-range ordering of the mineral phases of these two samples is caused by the nanocrystalline nature of apatite crystals in bone and teeth, which leads to a significant number of surface sites in slightly different environments,[80] by the presence of several substituting ions in the lattice, which favour a greater variety of chemical environments for the Ca^{2+} cations.

The EXAFS data of these three compounds was fitted to determine average Ca–O distances in the first-coordination sphere (Table S2). For HA, the data was fitted up to ~5 Å, showing that the average Ca–O distance in the first shell (2.43 Å) was in agreement with the experimental value.[8,79] In the case of HB and CT, fewer shells were considered because of the loss of long-range ordering. Nevertheless, the fits clearly showed that there is hardly any difference in the average Ca–O distances in the first shell of HB and CT (2.45 and 2.48 Å), and that these Ca–O distances are in the range expected from the ^{43}Ca NMR isotropic chemical shifts.

1c Local distortion around the calcium site. In contrast with other quadrupolar nuclei like sodium or magnesium, both experimental and computational studies of ^{43}Ca NMR parameters suggest that there is no strong correlation between ^{43}Ca P_Q values and the local structure around calcium.[52] Thus, the fact that the P_Q of HB is slightly larger than for CT (by ~10%, Table 1) does not necessarily mean that the calcium coordination environment in HB is slightly less symmetrical than in CT. In order to investigate in more detail the local distortions around calcium in these samples, Ca K-edge XANES spectra were recorded.

The general aspect of the Ca K-edge XANES spectra of HB and CT are similar to HA, which is not fully surprising given

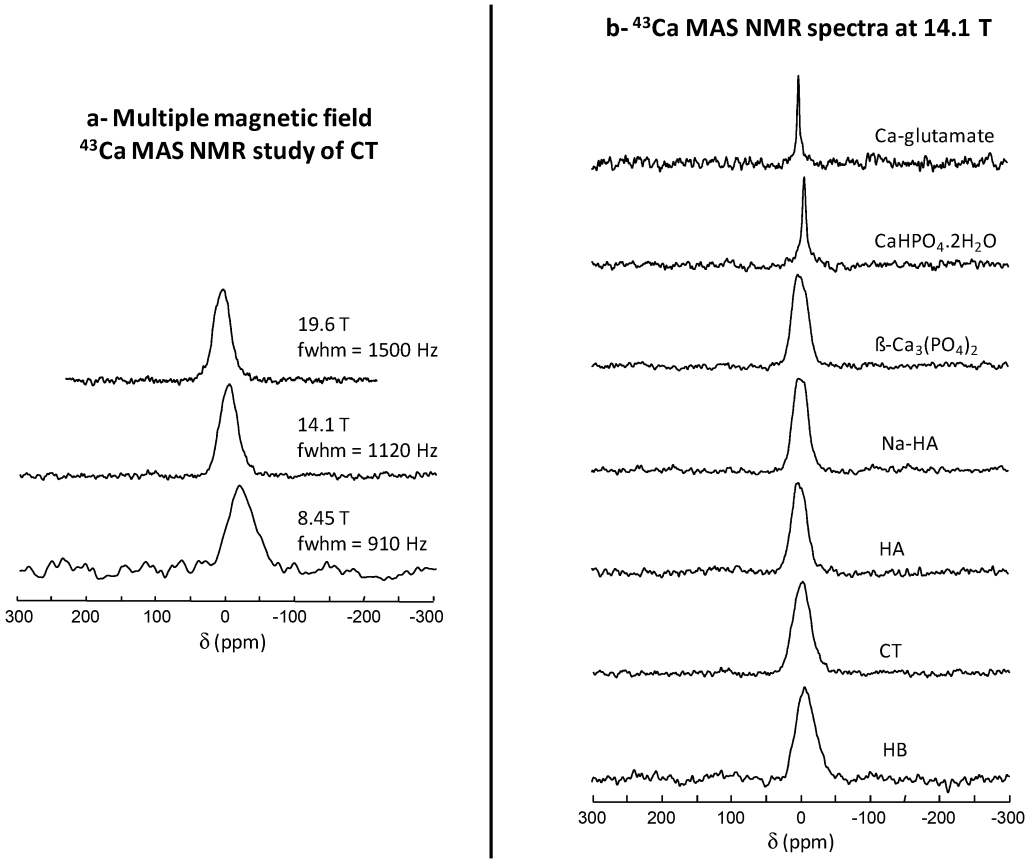

Fig. 2 (a) Natural abundance ^{43}Ca MAS NMR spectra of CT at 3 different magnetic fields. (b) Natural abundance ^{43}Ca MAS NMR spectra of HA, Na-HA, HB and CT at 14.1 T, and of some model compounds previously reported in the literature.[52,54,56]

Table 1 ^{43}Ca, ^{23}Na and ^{31}P NMR characteristics of CT, HB and synthetic sodium-substituted apatites

	CT	HB	Na-HA	Na-CO_3-HA[63]
^{43}Ca NMR				
P_Q (±0.2 MHz)[a]	2.1	2.3	—	—
δ_{iso} (±3.0 ppm)	3.0	3.4	—	—
^{23}Na NMR				
P_Q (±0.20 MHz)	1.37	1.58	1.65[b]	~1.2[c]
δ_{iso} (±3.0 ppm)	−1.7	−2.2	−0.1	−3.9
^{31}P NMR				
δ_{iso} (±0.1 ppm)	3.1	3.1	2.9	—

[a] For Na-HA, P_Q and δ_{iso} were not estimated, because the ^{43}Ca NMR spectra have only been recorded at 2 magnetic fields, and the 2 Ca sites are actually resolved at 19.6 T. For the data on non-substituted HA, see ref. 52 and 56. [b] For Na-HA, the P_Q value given must be considered with caution, given that the 2 sodium sites can be resolved by 3Q-MAS at 14.1 T. From the 3QMAS spectra, the δ_{iso} and P_Q values determined for these sites are {~1.6 ± 3.0 ppm; 1.4 ± 0.2 MHz} and {0.3 ± 3.0 ppm, 1.8 ± 0.2 MHz}, respectively. [c] For this sample, P_Q and δ_{iso} were determined from simulations of the ^{23}Na lineshapes obtained at two magnetic fields (see ref. 63).

that in the biological samples most of the calcium is in an apatite-like environment.[81,82] However, the XANES spectral features become less defined in the natural apatites (especially HB) because of the progressive loss of ordering of the mineral phase (Fig. 4). Interestingly, the intensity of the pre-edge is stronger for HB than CT. Given previous Ca K-edge XANES studies,[83] this suggests that the distortion around calcium is slightly greater in the bone. Thus, the larger value of P_Q in HB compared to CT could well reflect in this particular case the degree of local symmetry around the cation.

Although it appears at this stage that Ca K-edge XANES is a more sensitive probe of the average local distortions around calcium sites in natural apatites than ^{43}Ca P_Q values, the very small differences in the ^{43}Ca P_Q values seem to agree with the conclusions from the XANES spectra. Thus, it would be worth carrying out additional ^{43}Ca NMR and Ca K-edge XANES experiments on a wider range of natural apatites, to see whether P_Q parameters can indeed be considered as valuable structural indicator of the local distortion at calcium sites for these samples.

1d Distribution in calcium local environments

As previously mentioned, the Ca K-edge EXAFS spectra of HB and CT show that there is a loss of long-range ordering around the calcium. The evolution of the overall ^{43}Ca NMR linewidths with the magnetic field provides additional insight into the "disorder" around calcium sites. Indeed, although the overall linewidths of HB and CT are systematically greater than for HA[56] and Na-HA, their variation with the magnetic field is different: the ^{43}Ca linewidths for HB and CT systematically increase with the magnetic field, despite the fact that the second-order quadrupolar broadening, which scales as $(1/\nu_0)$, is becoming smaller.[51] This suggests that there is a

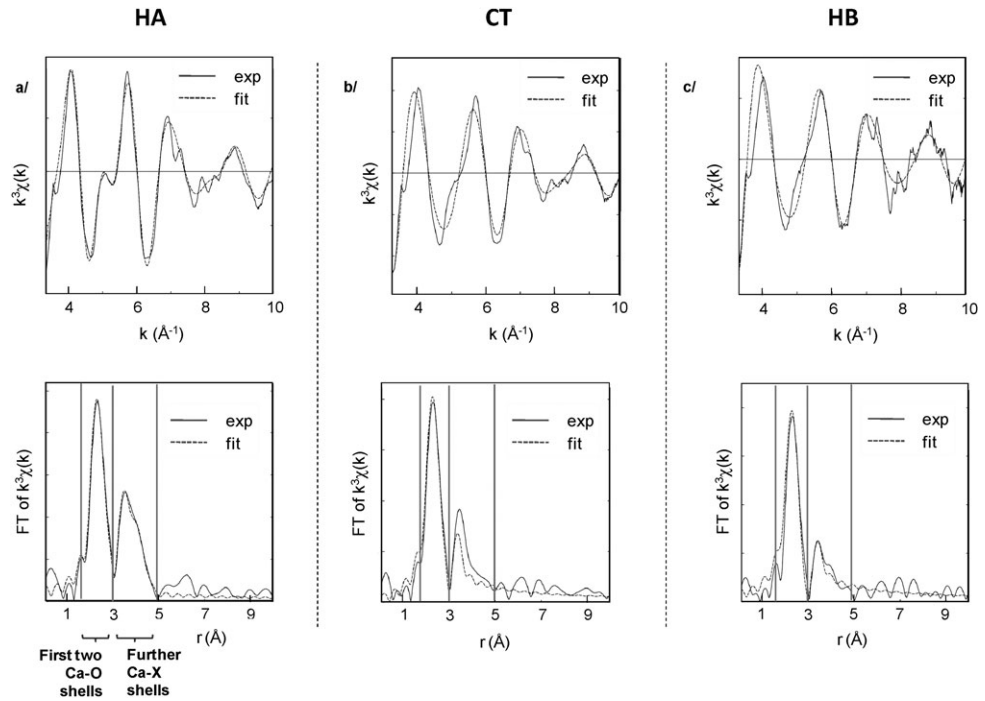

Fig. 3 Ca K-edge EXAFS spectra and moduli of the Fourier transforms of HA, CT and HB. Fits were performed considering 8 shells for HA, and 3 for HB and CT (see Supplementary Table S2 for details).

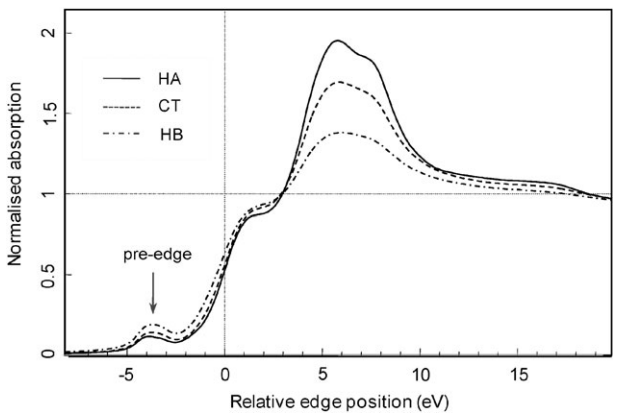

Fig. 4 Expansion of the edge region of the Ca K-edge XANES spectra of HA, HB and CT. (No clear differences in the XANES spectra appear beyond 20 eV.)

larger ^{43}Ca chemical shift dispersion in HB and CT,[51,56,84] which could arise from the loss of long-range ordering observed in Ca K-edge EXAFS spectra, and also from the presence of several non-apatitic calcium environments. Indeed, as shown in Fig. 2 and S6, the ^{43}Ca NMR signals of HB and CT cover a range of chemical shifts in which the signals of several other calcium phosphates and hydrogenphosphates might appear (which could model other environments of calcium in bone and tooth minerals, such as fluoroapatite), and of calcium-carboxylates (like Ca-glutamate—a compound which could model the environment of Ca^{2+} ions interacting with carboxylate groups at the surface of apatite).[50,85]

In order to reach a clearer picture of the different calcium environments in bone, it appears necessary to determine the relative positions of the neighbouring nuclei. This is not possible using EXAFS, because of the significant loss of long-range ordering beyond the first 2 shells, and of the presence of several back-scatterers in these shells. In contrast, solid state NMR is well suited to determine proximities between nuclear spins in disordered and non-crystalline samples, and examples of ^{43}Ca···^{1}H correlation experiments have been reported.[86,87] A preliminary experiment was thus carried out on HB to try to evidence differences in Ca···H environments, using the ^{43}Ca{^{1}H} REDOR sequence. As shown in Fig. S7, it seems that there are slight changes in the ^{43}Ca spectrum when the ^{1}H dipolar coupling is reintroduced. Nevertheless, this would deserve confirmation, because the signal-to-noise ratio is still very low, even after 2 days of acquisition per spectrum at 14.1 T. It can be predicted that with the increase in magnetic fields and the development of signal-enhancement sequences, such experiments should become increasingly used as sources of improved information about calcium environments in these samples.

2 ^{23}Na NMR investigation

2a Multiple magnetic field ^{23}Na MAS NMR experiments. Despite the low concentration of sodium in the samples (<1.4 wt% for HB and CT), ^{23}Na MAS NMR spectra of HB, CT and Na-HA could be obtained in very reasonable experimental times (~30 min at 14.1 T, using a 4 mm o.d. rotor). The spectra were thus recorded at four magnetic fields. For all compounds, a slightly asymmetric lineshape was observed with a tailing towards low frequencies, but with no resolution of multiple sites, and broader signals for HB and CT (Fig. 5 and S8).[88]

As in the ^{43}Ca NMR study, by plotting δ_{max} as a function of $(1/\nu_0)^2$ (where ν_0 is the ^{23}Na Larmor frequency), average

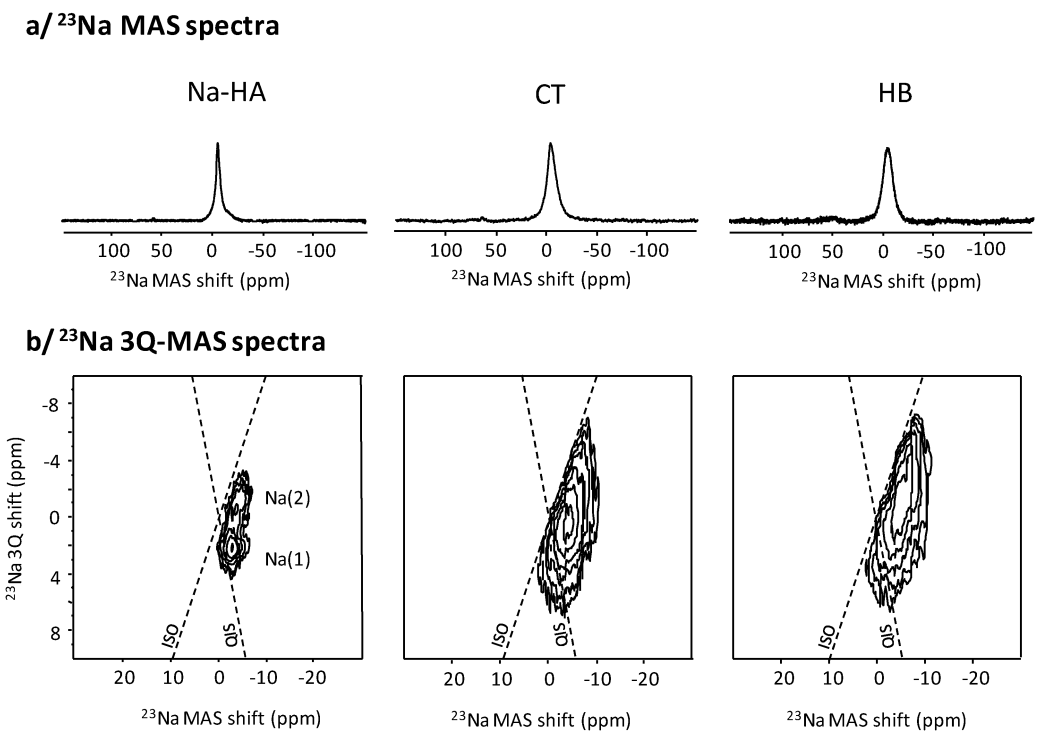

Fig. 5 ^{23}Na MAS NMR spectra and 3Q-MAS NMR sheared spectra of Na-HA, CT and HB at 14.1 T.

^{23}Na δ_{iso} and P_Q values were determined using eqn (1), with $F(I)$ equal to 1/3 for $I = 3/2$.[78] Results are given in Table 1, alongside those previously reported for a synthetic Na-carbonated apatite.[63] The ^{23}Na δ_{iso} and P_Q parameters of HB and CT are very similar to those found for the two synthetic compounds, which suggests that sodium is in similar environments. Furthermore, these values are in the range of those previously reported for sodium phosphates and hydrogen-phosphates.[89–94] However, at this stage, it is difficult to extract any further information from δ_{iso}, because previous studies have shown that for compounds in which sodium has exclusively oxygen atoms as nearest neighbours, ^{23}Na isotropic shifts depend on the valence *and* Na–O distances of the closest oxygen atoms, both of which are unknown here.[92,95] Although Na K-edge EXAFS[96] and XANES[97] might provide additional insight into the Na···O coordination environment, such experiments are expected to be very difficult to carry out because of the low sodium content in the samples. In contrast, high resolution ^{23}Na solid state NMR experiments, and in particular correlation experiments, may be used even at these low sodium concentrations to investigate the sodium environment in HB and CT.

2b High resolution NMR analysis of Na environments. The two-dimensional 3Q (triple quantum)-MAS spectra of Na-HA, HB and CT were recorded at 14.1 T (Fig. 5b), to achieve better resolution of the ^{23}Na NMR signals. In the case of Na-HA, two distinct contour signals were clearly resolved, thus indicating that there are two different sodium sites. However, no well-defined quadrupolar lineshape was observed on the 1D-MAS projections, meaning that there are distributions in the local environment of sodium in each site. In the case of HB and CT, no resolution of multiple sites was observed by 3Q-MAS, and the size and position of the crosspeaks show that *both* the ^{23}Na chemical shifts and quadrupolar parameters are distributed, which is not surprising given the complexity and lower crystallinity of these materials.

Because of the high natural abundance of ^{23}Na, heteronuclear NMR correlation experiments can be more easily achieved for ^{23}Na than ^{43}Ca, and several studies of ^{23}Na–^{31}P and ^{23}Na–^{1}H proximities have been reported for both crystalline and amorphous materials.[98–100] ^{23}Na{^{31}P} REDOR experiments were thus carried out on the samples, in order to investigate the different sodium–phosphorus through space correlations. In each case, an overall decrease of the ^{23}Na lineshape was observed in the presence of ^{31}P recoupling pulses, which indicates that all the sodium is located close to phosphates (Fig. 6a). For Na-HA, which is a crystalline apatite phase, this means that the two sodium sites resolved by 3Q-MAS correspond to Na^+ substitutions within the apatite lattice. For HB and CT, the overall dephasing of the ^{23}Na signal indicates that at least some of the sodium is in the apatite phase. However, some sodium could also be located in other non-crystalline calcium-phosphate phases such as amorphous calcium phosphate, which have been shown to be present in bone (at least at the early stages of mineralisation).[8]

In order to further analyse the sodium environment in these samples, experiments aiming at looking at differences in sodium-proton proximities were carried out. The two-dimensional ^{1}H{^{23}Na} R^3-HMQC NMR spectra of Na-HA, HB and CT were recorded, as this sequence is well-adapted to the investigation of dipolar couplings between spin-1/2 and quadrupolar nuclei (Fig. 7).[73,87] In the case of Na-HA, a cross-peak is observed between the ^{1}H signal characteristic

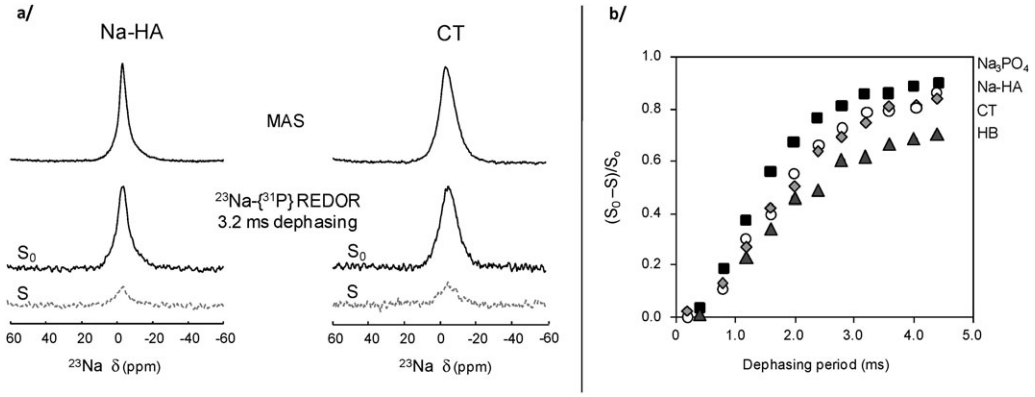

Fig. 6 (a) ^{23}Na NMR spectra of Na-HA and CT: MAS spectrum (top), ^{23}Na{^{31}P} REDOR study after a 3.2 ms dephasing period (spin-echo control spectrum S_0*vs.* REDOR spectrum S). (b) ^{23}Na{^{31}P} REDOR build-up for HB (△), CT (◊), Na-HA (○) and $Na_3(PO_4)$ (■).

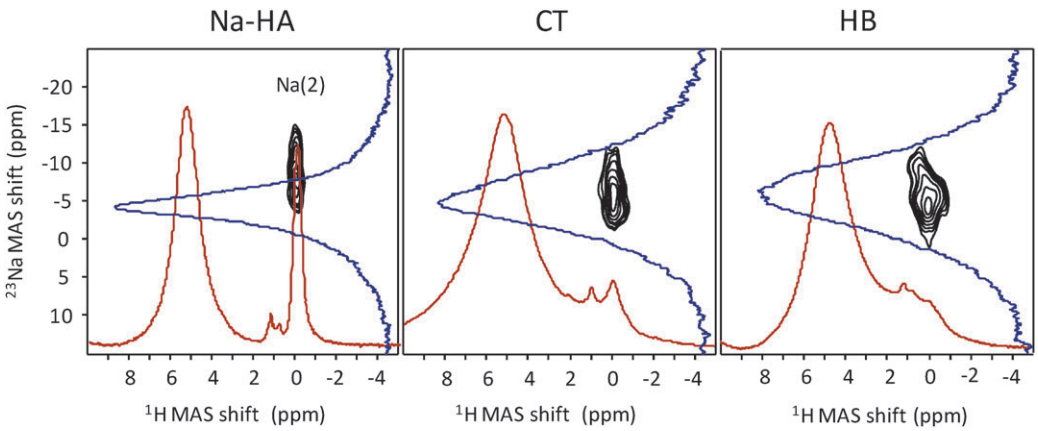

Fig. 7 ^{1}H{^{23}Na} R^3-HMQC NMR spectra of Na-HA, CT and HB, recorded at 14.1 T. The ^{1}H and ^{23}Na MAS NMR spectra are overlayed in each dimension.

of the apatite OH group (at 0 ppm) and the low frequency component of the ^{23}Na MAS signal, which means that it corresponds to sodium cations close to the OH (*i.e.* in the "M(2)" crystallographic site of HA, shown in Fig. 1), and thus that the high frequency sodium site observed in 3Q-MAS corresponds to sodium in the "M(1)" site.[101] In the case of HB and CT, a strong cross peak also correlates the ^{23}Na NMR signal to a ^{1}H signal at ~0 ppm, thereby demonstrating that Na^+ substitutes in the M(2) calcium site (at least) in these samples.[102] It is noteworthy that the shapes of the cross peaks observed on the ^{1}H{^{23}Na} R^3-HMQC spectra of HB and CT show that the distribution in chemical shift around sodium is larger than for Na-HA, in agreement with the 3QMAS experiments.

The presence of Na^+ inside the apatite phase of HB and CT is not fully surprising given that previous studies of crystalline Na-substituted calcium-phosphate phases have shown that Ca^{2+} is readily replaced by Na^+ in phosphates,[63,98] despite the difference in charge between the two cations. Such a situation is likely to be related to the close similarity between ionic radii of Na^+ and Ca^{2+} (1.02 Å *vs.* 1.00 Å),[103] leading to similar average M···O bond distances in sodium and calcium phosphates (~2.42 ± 0.70 Å for M = Na,[104] *vs.* ~2.45 ± 0.60 Å for M = Ca).[52] Interestingly, the ^{23}Na NMR parameters of HB and CT are very similar, as well as their 3QMAS and ^{1}H{^{23}Na} R^3-HMQC spectra. However, this does not mean that the "average" sodium environment in these samples is identical. Indeed, as shown in Fig. 6b, differences can be evidenced in their ^{23}Na{^{31}P} REDOR build-up profiles. Although at this stage, such differences cannot be interpreted unambiguously, notably because they involve complicated Na–P multiple spin systems, they could well reflect differences in charge balancing mechanisms related to the substitution of Ca^{2+} by Na^+ (because PO_4^{3-} anions can be replaced by HPO_4^{2-} or CO_3^{2-})[105] and/or in crystallinity and number of surface sites between the mineral phases. Indeed, the Na–P dipolar buildups of CT and Na-HA are very similar (Fig. 6b), in line with the presence of mineral particles in CT which are on average larger and more crystalline than in HB (Fig. S1). Additional ^{23}Na{^{31}P} REDOR studies would deserve to be carried out to further investigate this point, by comparing the build-up profiles of several natural apatites with those of Na-substituted synthetic analogues of different crystallinity and surface area, and also of sodium-phosphates of known structure such as Na_3PO_4, for which the average ^{23}Na–^{31}P dipole second moment couplings (which inform on the average Na···P distances) have already been determined.[106] Furthermore,

given that some studies suggest that HPO_4^{2-} and Na^+ ions are preferentially located at the surface of bone apatite crystals,[11,28,29] such REDOR build-up profiles could actually become a new tool to understand the surface structures of mineral particles in bone, which is important for understanding the structure of the mineral–organic interface. As a result, we anticipate that $^{23}Na\{^{31}P\}$ REDOR experiments such as those presented here (or, alternatively, C-REDOR experiments, which are more adapted to study heteronuclear dipolar couplings in multiple spin systems),[107] as well as additional ^{23}Na–^{1}H correlation experiments, should help provide some answers to these questions.

Conclusion

This work has demonstrated that the local environment of both calcium and sodium cations in naturally-occurring bone and teeth can be analysed by solid state NMR. In the case of calcium, the main cation present in bone mineral, we have reported the first ^{43}Ca NMR spectra of bone mineral. These allow the average Ca–O distance to be estimated from the ^{43}Ca isotropic chemical shifts, and complement well studies of calcium local environments by Ca K-edge EXAFS and XANES.

In the case of sodium, ^{23}Na–^{1}H and ^{23}Na–^{31}P NMR correlation experiments have been performed in reasonable timescales, providing the first direct evidence that some sodium is located inside the apatite lattice in bone and teeth, and that there is a wider distribution in local sodium environments compared to synthetic Na-substituted HA. With the current instrumental advances, notably the development of higher magnetic fields and the design of more efficient probes, it can be expected that an even better description of the sodium environment in these samples will soon be reached. For instance, correlation experiments would be worth looking into in more detail on smaller volumes of sample, using for example ultra-fast MAS probes, in order to understand better the structure around sodium in bone and teeth, and see whether there are any changes from one part of bone to the other. Furthermore, it should be possible to differentiate the distributions in chemical shift and quadrupolar parameters using two-dimensional experiments such as MQ double-rotation (DOR).[108] Such ^{23}Na NMR studies of bone and teeth are expected to develop rapidly in the near future, as they should lead to a better description and understanding of the unique structure of natural apatite samples, and also help shed light on bone remodeling mechanisms.

Acknowledgements

This work was supported by BBSRC, EPSRC, and the University of Warwick. AW would like to thank NSERC for a Canadian PDF, and DL the 6th European Community Framework Program for a Marie Curie IEF. ELETTRA (proposal 2007512) and the European Community (EU contract RII3-CT-2004-506008-IA-SFS) are acknowledged for financial support, and Dr Andrea Cognigni and Dr Luca Olivi are thanked for their help on the XAFS beamline. The NHMFL in Tallahassee is acknowledged for experimental time on the high field 19.6 T NMR magnet. Prof. Ray Dupree is thanked for many fruitful discussions on this work, and Dr Lijiang Song for performing the ICP-MS measurements.

References

1 S. Weiner and W. Traub, *FASEB J.*, 1992, **6**, 879.
2 S. Weiner and H. D. Wagner, *Annu. Rev. Mater. Sci.*, 1998, **28**, 271.
3 M. J. Glimcher, *Rev. Mineral. Geochem.*, 2006, **64**, 223.
4 L. Wang, G. H. Nancollas, Z. J. Henneman, E. Klein and S. Weiner, *Biointerphases*, 2006, **1**, 106.
5 H. Gao, B. Ji, L. J. Ingomar, E. Arz and P. Fratzl, *Proc. Natl. Acad. Sci. U. S. A.*, 2003, **100**, 5597.
6 V. Benezra Rosen, L. W. Hobbs and M. Spector, *Biomaterials*, 2002, **23**, 921.
7 M. A. Rubin, J. Rubin and I. Jasiuk, *Bone*, 2004, **35**, 11.
8 J. C. Elliott, *Structure and Chemistry of the Apatites and other Calcium Phosphates*, Elsevier, Amsterdam, 1994.
9 S. V. Dorozhkin, *J. Mater. Sci.*, 2007, **42**, 1061.
10 N. B. Roberts, H. P. J. Walsh, L. Klenerman, S. A. Kelly and T. R. Helliwell, *J. Anal. At. Spectrom.*, 1996, **11**, 133.
11 R. P. Heaney, *J. Am. Coll. Nutr.*, 2006, **25**, 271S.
12 R. K. Rude, H. E. Gruber, L. Y. Wei, A. Frausto and B. G. Mills, *Calcif. Tissue Int.*, 2003, **72**, 32.
13 J. D. B. Featherstone, *Community Dent. Oral Epidemiol.*, 1999, **27**, 31.
14 C. Rey, M. Shimizu, B. Collins and M. J. Glimcher, *Calcif. Tissue Int.*, 1991, **49**, 383.
15 E. P. Paschalis, F. Betts, E. DiCarlo, R. Mendelsohn and A. L. Boskey, *Calcif. Tissue Int.*, 1997, **61**, 480.
16 S. Takata, A. Shibata, H. Yonezu, T. Yamada, M. Takahashi, A. Abbaspour and N. Yasui, *J. Med. Inv.*, 2004, **51**, 133.
17 R. G. Handschin and W. B. Stern, *Bone*, 1995, **16**, S355.
18 R. G. Handschin and W. B. Stern, *Calcif. Tissue Int.*, 1992, **51**, 111.
19 N. Binsted, S. S. Hasnain and D. W. L. Hukins, *Biochem. Biophys. Res. Commun.*, 1982, **107**, 89.
20 J. E. Harries, D. W. L. Hukins and S. S. Hasnain, *Calcif. Tissue Int.*, 1988, **43**, 250.
21 F. Peters, K. Schwarz and M. Epple, *Thermochim. Acta*, 2000, **361**, 131.
22 A. H. Roufosse, W. P. Aue, J. E. Roberts, M. J. Glimcher and R. G. Griffin, *Biochemistry*, 1984, **23**, 6115.
23 M. E. Ebifegha, R. F. Code, K. G. McNeill and M. Szyjkowski, *Can. J. Phys.*, 1986, **64**, 282.
24 W. Kolodziejski, *Top. Curr. Chem.*, 2005, **246**, 235 (and references therein).
25 A. Kaflak and W. Kolodziejski, *Magn. Reson. Chem.*, 2008, **46**, 335.
26 J. Kolmas and W. Kolodziejski, *Chem. Commun.*, 2007, 4390.
27 J. Kolmas, A. Slosarczyk, A. Wojtowicz and W. Kolodziejski, *Solid State Nucl. Magn. Reson.*, 2007, **32**, 53.
28 A. Kaflak and W. Kolodziejski, *Solid State Nucl. Magn. Reson.*, 2007, **31**, 174.
29 S. Maltsev, M. J. Duer, R. C. Murray and C. Jaeger, *J. Mater. Sci.*, 2007, **42**, 8804.
30 A. Kaflak-Hachulska, A. Samoson and W. Kolodziejski, *Calcif. Tissue Int.*, 2003, **73**, 476.
31 Y. Wu, J. L. Ackerman, E. S. Strawich, C. Rey, H.-M. Kim and M. J. Glimcher, *Calcif. Tissue Int.*, 2003, **72**, 610.
32 Y. Wu, J. L. Ackerman, H.-M. Kim, C. Rey, A. Barroug and M. J. Glimcher, *J. Bone Miner. Res.*, 2002, **17**, 472.
33 A. P. Legrand, B. Bresson and J.-M. Bouler, *Key Eng. Mater.*, 2001, **192**, 759.
34 A. Kaflak, D. Chmielewski, A. Gorecki and W. Kolodziejski, *Solid State Nucl. Magn. Reson.*, 1998, **10**, 191.
35 C. Ramanathan, Y. Wu, B. Pfleiderer, M. J. Lizak, L. Garrido and J. L. Ackerman, *J. Magn. Reson., Ser. A*, 1996, **121**, 127.
36 Y. Wu, M. J. Glimcher, C. Rey and J. L. Ackerman, *J. Mol. Biol.*, 1994, **244**, 423.
37 J. E. Roberts, L. C. Bonar, R. G. Griffin and M. J. Glimcher, *Calcif. Tissue Int.*, 1992, **50**, 42.

38 L. C. Bonar, M. Shimizu, J. E. Roberts, R. G. Griffin and M. J. Glimcher, *J. Bone Miner. Res.*, 1991, **6**, 1167.
39 G. Cho, Y. Wu and J. L. Ackerman, *Science*, 2003, **300**, 1123.
40 E. R. Wilson, A. Awonusi, M. D. Morris, D. H. Kohn, M. M. J. Tecklenburg and L. W. Beck, *Biophys. J.*, 2006, **90**, 3722.
41 E. R. Wilson, A. Awonusi, M. D. Morris, D. H. Kohn, M. M. J. Tecklenburg and L. W. Beck, *J. Bone Miner. Res.*, 2005, **20**, 625.
42 L. T. Kuhn, M. D. Grynpas, C. C. Rey, Y. Wu, J. L. Ackerman and M. J. Glimcher, *Calcif. Tissue Int.*, 2008, **83**, 146.
43 Y.-H. Tseng, Y.-L. Tsai, T. W. T. Tsai, J. C. H. Chao, C.-P. Lin, S.-H. Huang, C.-Y. Mou and J. C. C. Chan, *Chem. Mater.*, 2007, **19**, 6088.
44 K. Beshah, C. Rey, M. J. Glimcher, M. Sgimizu and R. G. Griffin, *J. Solid State Chem.*, 1990, **84**, 71.
45 S. P. Gabuda, A. A. Gaidash, S. G. Kozlova and N. L. Allan, *J. Struct. Chem.*, 2006, **47**, 258.
46 N. Gelman and R. F. Code, *J. Magn. Reson.*, 1992, **96**, 290.
47 R. F. Code, N. Gelman, R. L. Armstrong, R. S. Hallsworth, C. Lemaire and P. T. Cheng, *Phys. Med. Biol.*, 1990, **35**, 1271.
48 D. G. Reid, M. J. Duer, R. C. Murray and E. R. Wise, *Chem. Mater.*, 2008, **20**, 3549.
49 E. R. Wise, S. Maltsev, M. E. Davies, M. J. Duer, C. Jaeger, N. Loveridge, R. C. Murray and D. G. Reid, *Chem. Mater.*, 2007, **19**, 5055.
50 C. Jaeger, N. S. Groom, E. A. Bowe, A. Homer, M. E. Davies, R. C. Murray and M. J. Duer, *Chem. Mater.*, 2005, **17**, 3059.
51 K. J. D. MacKenzie and M. E. Smith, *Multinuclear Solid State NMR of Inorganic Materials*, Pergamon, Oxford, 2002.
52 C. Gervais, D. Laurencin, A. Wong, F. Pourpoint, B. Woodward, A. P. Howes, K. J. Pike, R. Dupree, F. Mauri, C. Bonhomme and M. E. Smith, *Chem. Phys. Lett.*, 2008, **464**, 42.
53 G. M. Bowers and R. J. Kirkpatrick, *J. Am. Ceram. Soc.*, 2009, **92**, 545.
54 A. Wong, D. Laurencin, G. Wu, R. Dupree and M. E. Smith, *J. Phys. Chem. A*, 2008, **112**, 9807.
55 D. L. Bryce, E. B. Bultz and D. Aebi, *J. Am. Chem. Soc.*, 2008, **130**, 9282.
56 D. Laurencin, A. Wong, R. Dupree and M. E. Smith, *Magn. Reson. Chem.*, 2008, **46**, 347.
57 R. E. Youngman and C. M. Smith, *Phys. Rev. B: Condens. Matter Mater. Phys.*, 2008, **78**, 014112.
58 I. C. M. Kwan, A. Wong, Y.-M. She, M. E. Smith and G. Wu, *Chem. Commun.*, 2008, 682.
59 K. J. D. MacKenzie, M. E. Smith and A. Wong, *J. Mater. Chem.*, 2007, **17**, 5090.
60 A. Wong, A. P. Howes, R. Dupree and M. E. Smith, *Chem. Phys. Lett.*, 2006, **427**, 201–205.
61 F. J. Rühli, T. Böni, J. Perlo, F. Casanova, M. Baias, E. Egarter and B. Blümich, *J. Cult. Herit.*, 2007, **8**, 257.
62 P. Rong, R. R. Regatte and A. Jerschow, *J. Magn. Reson.*, 2008, **193**, 207.
63 H. E. Mason, A. Kozlowski and B. L. Phillips, *Chem. Mater.*, 2008, **20**, 294.
64 E. Bertoni, A. Bigi, G. Cojazzi, M. Gandolfi, S. Panzavolta and N. Roveri, *J. Inorg. Biochem.*, 1998, **72**, 29.
65 This sample, purchased from Aldrich, was labeled as "hydroxylapatite-$3Ca_3(PO_4)_2.Ca(OH)_2$" (catalog # 28,939-6, lot # 06616CS). However, it appeared to also contain Na^+ (according to EDXS), as well as HPO_4^{2-} ions (according to ^1H and ^{31}P solid state NMR and IR). The synthetic route chosen to prepare this sample was not revealed by Aldrich; however, it can be suspected that the presence of sodium comes from the use of NaH_2PO_4 or NaOH at some point during the synthesis. It is noteworthy that contrary to the Na-substituted carbonated HA on which ^{23}Na NMR studies have recently been performed (see ref. 63), there is no significant concentration of carbonates in Na-HA, as evidenced from the absence of strong C–O stretching vibrations between 1300 and 1400 cm^{-1} (Fig. S1).
66 R. Siegel, T. T. Nakashima and R. E. Wasylishen, *Concepts Magn. Reson.*, 2005, **26a**, 47.
67 K. T. Kwak, S. Prasad, T. Clark and P. J. Grandinetti, *Solid State Nucl. Magn. Reson.*, 2003, **24**, 71.
68 E. van Veenendaal, B. H. Meier and A. P. M. Kentgens, *Mol. Phys.*, 1998, **93**, 195.
69 B. Ravel and M. Newville, *J. Synchrotron Radiat.*, 2005, **12**, 537.
70 K. V. Klementev, *VIPER for Windows*, freeware: www.desy.de/~klmn/viper.html; K. V. Klementev, *J. Phys. D: Appl. Phys.*, 2001, **34**, 209.
71 N. Binsted, J. W. Campbell, S. J. Gurman and P. C. Stephenson, *EXAFS Analysis programs*, Daresbury Laboratory, Warrington, UK.
72 L. Frydman and J. S. Harwood, *J. Am. Chem. Soc.*, 1995, **117**, 5367.
73 J. P. Amoureux and C. Fernandez, *Solid State Nucl. Magn. Reson.*, 1998, **10**, 211.
74 T. Gullion and J. Schaefer, *Adv. Magn. Reson.*, 1989, **13**, 57.
75 T. Gullion and J. Schaefer, *J. Magn. Reson.*, 1989, **81**, 196.
76 T. Gullion, D. B. Baker and M. S. Conradi, *J. Magn. Reson.*, 1990, **89**, 479.
77 J. Trébosc, B. Hu and J. P. Amoureux, *J. Magn. Reson.*, 2007, **186**, 220.
78 Strictly, the centre of gravity of the signal δ_{CG} should be considered (see ref. 51). However, given that the lineshapes are featureless and nearly symmetric, these are effectively synonymous here.
79 J. E. Harries, D. W. L. Hukins and S. S. Hasnain, *J. Phys. C: Solid State Phys.*, 1986, **19**, 6859.
80 H. Chappell, M. Duer, N. Groom, C. Pickard and P. Bristowe, *Phys. Chem. Chem. Phys.*, 2008, **10**, 600.
81 D. Eichert, M. Salome, M. Banu, J. Susini and C. Rey, *Spectrochim. Acta, Part B*, 2005, **60**, 850.
82 F. E. Sowrey, L. J. Skipper, D. M. Pickup, K. O. Drake, Z. Lin, M. E. Smith and R. J. Newport, *Phys. Chem. Chem. Phys.*, 2004, **6**, 188.
83 D. R. Neuville, L. Cormier, A.-M. Flank, V. Briois and D. Massiot, *Chem. Geol.*, 2004, **213**, 153.
84 S. C. Kohn, R. Dupree and M. E. Smith, *Geochim. Cosmochim. Acta*, 1989, **53**, 2925.
85 Q. Q. Hoang, F. Sicheri, A. J. Howard and D. S. C. Yang, *Nature*, 2003, **425**, 977.
86 D. Laurencin, A. Wong, R. Dupree, J. V. Hanna and M. E. Smith, *J. Am. Chem. Soc.*, 2008, **130**, 2412.
87 A. Wong, D. Laurencin, R. Dupree and M. E. Smith, *Solid State Nucl. Magn. Reson.*, 2009, **35**, 32.
88 It is noteworthy that at 14.1 T, the ^{23}Na MAS NMR linewidth at half-maximum of the signals is only reduced by ~30 Hz when increasing the spinning speed from 5 to 10 kHz, while the position of the maximum remains the same.
89 C. A. Fyfe, H. Meyer zu Altenschildesche and J. Skibsted, *Inorg. Chem.*, 1999, **38**, 84.
90 M. Baldus, B. H. Meier, R. R. Ernst, A. P. M. Kentgens, H. Meyer zu Altenschildesche and R. Nesper, *J. Am. Chem. Soc.*, 1995, **117**, 5141.
91 C. Johnson, E. A. Moore and M. Mortimer, *Chem. Commun.*, 2000, 791.
92 H. Koller, G. Engelhardt, A. P. M. Kentgens and J. Sauer, *J. Phys. Chem.*, 1994, **98**, 1544.
93 A. Medek, J. S. Harwood and L. Frydman, *J. Am. Chem. Soc.*, 1995, **117**, 12779.
94 I. Abrahams, K. Franks, G. E. Hawkes, G. Philippou, J. Knowles, P. Bodart and T. Nunes, *J. Mater. Chem.*, 1997, **7**, 1573.
95 A. Wong and G. Wu, *J. Phys. Chem. A*, 2000, **104**, 11844.
96 D. A. McKeown, G. A. Waychunas and G. E. Brown Jr, *J. Non-Cryst. Solids*, 1985, **74**, 325.
97 L. Cormier and D. R. Neuville, *Chem. Geol.*, 2004, **213**, 103.
98 L. Obadia, P. Deniard, B. Alonso, T. Rouillon, S. Jobic, J. Guicheux, M. Julien, D. Massiot, B. Bujoli and J.-M. Bouler, *Chem. Mater.*, 2006, **18**, 1425–1433.
99 D. P. Lang, T. M. Alam and D. N. Bencoe, *Chem. Mater.*, 2001, **13**, 420.
100 A. Goldbourt, E. Vinogradov, G. Goobes and S. Vega, *J. Magn. Reson.*, 2004, **171**, 10.
101 A one-dimensional $^{23}Na\{^1H\}$ 3Q-REDOR experiment also leads to the same assignment of the 2 sodium sites of Na-HA, as only the low frequency Na(2) component is affected by ^1H recoupling pulses (see Fig. S9).
102 It is noteworthy that some of the sodium might also be located close to other "protons" in bone and teeth, and for example near

mobile water molecules. These environments do not appear on the HMQC spectra reported here.
103 R. D. Shannon, *Acta Crystallogr., Sect. A: Cryst. Phys., Diffr., Theor. Gen. Cryst.* , 1976, **32**, 751.
104 This average value was determined from the crystal structures of sodium phosphates and hydrogen-phosphates on which ^{23}Na experiments have been carried out (see ref. 89–93).
105 Y. Pan and M. E. Fleet, *Rev. Mineral. Geochem.*, 2002, **48**, 13.
106 J. C. C. Chan and H. Eckert, *J. Magn. Reson.*, 2000, **147**, 170.
107 J. C. C. Chan, *Chem. Phys. Lett.*, 2001, **335**, 289.
108 I. Hung, A. Wong, A. P. Howes, T. Anupõld, A. Samoson, M. E. Smith, D. Holland, S. P. Brown and R. Dupree, *J. Magn. Reson.*, 2009, **197**, 229.